Journal of Power Sources 240 (2013) 281–293

Contents lists available at SciVerse ScienceDirect

Journal of Power Sources

journal homepage: www.elsevier.com/locate/jpowsour

Review

Study of proton exchange membrane fuel cells using electrochemical impedance spectroscopy technique – A review

Seyed Mohammad Rezaei Niya, Mina Hoorfar*

University of British Columbia, School of Engineering, Kelowna, V1V 1V7 BC, Canada

HIGHLIGHTS

- Electrochemical impedance spectroscopy in diagnosing PEM fuel cells is reviewed.
- The EIS technique and various equivalent circuit elements are discussed.
- Modifications to impedance measurements and interpretations are presented.
- Critical points misinterpreted in the EIS measurement models are discussed.

GRAPHICAL ABSTRACT

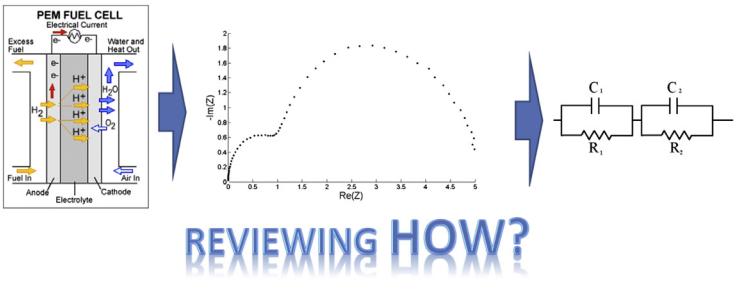

ARTICLE INFO

Article history:
Received 16 July 2012
Received in revised form
1 March 2013
Accepted 3 April 2013
Available online 1 May 2013

Keywords:
Electrochemical impedance spectroscopy (EIS)
Proton exchange membrane fuel cell (PEMFC)
Fuel cell modeling
Equivalent circuit

ABSTRACT

Electrochemical impedance spectroscopy (EIS) technique is well established in recent years to study and diagnose proton exchange membrane fuel cells (PEMFC). In this paper, the recent published research results in this field are reviewed. The EIS technique and equivalent circuit concept are introduced and recent applications of EIS in PEM fuel cell modeling and diagnosis are thoroughly reviewed. The paper also includes outstanding improvements conducted in EIS measurement and hardware. Finally the critical points that can be misinterpreted in the EIS measurement models in the field of PEM fuel cells are discussed.

1. Introduction

High dependency of conventional power generators to fossil fuels which has resulted in global warming and environmental pollution in the recent decades have motivated the research and development toward new, clean, inexpensive and robust power generation devices. Among them, fuel cells have been accepted as a prospective alternative for nowadays sources of energy. The fuel cell has considerably high power density with no emission or any moving parts. This increases the potential of being a reliable and robust system for long-term usage. Also, compared to batteries, the power (i.e., proportional to the fuel cell size) and capacitance (i.e., proportional to the reservoir size) characteristics of fuel cells are independent, and hence they can be employed in a wide range of applications [1]. Despite the general success made toward the advancement of fuel cells, their performance and applicability are limited due to several factors. In essence, the final cost of a fuel cell is the major barrier for commercialization.

* Corresponding author. Tel.: +1 250 807 8804; fax: +1 250 807 9850.
E-mail address: mina.hoorfar@ubc.ca (M. Hoorfar).

0378-7753/$ – see front matter © 2013 Elsevier B.V. All rights reserved.
http://dx.doi.org/10.1016/j.jpowsour.2013.04.011

Also, the best fuel for the low temperature fuel cells is hydrogen that has low volumetric energy density and is hard to store. Hydrogen has to be completely pure (especially in proton exchange membrane fuel cells) and alternative fuels usually need reforming [1]. Moreover, robustness and durability under start–stop cycles are not reliable in the current form of the fuel cells as has been indicated in the strategic planning of US department of energy (DOE) which is directed toward the development of a portable power fuel cell system (<250 W) with an energy density of 900 Wh L^{-1} by 2015, a transportation fuel cell system with 5000-h durability by 2017, and a micro-CHP (Combined Heat and Power) fuel cell system (5 kW) with 60,000-h durability and a medium-scale CHP fuel cell system (100 kW–3 MW) with 80,000-h durability by 2020 [2].

Among various kinds of fuel cells, a proton exchange membrane fuel cell (PEMFC) which performs at low operating temperature and relatively high power density has captured the most attention. In PEMFC, the hydrogen gas is fed into the anode; while usually the air (or pure oxygen) is fed to the cathode. The hydrogen is split into the electron and positive ions which move through a proton-conducting membrane to the anode. The transported protons are combined with the oxygen in the cathode, producing water as by-product. The balance in the water transport through and out of the cell is very crucial to avoid flooding and dehydration of the membrane.

There are different electrochemical methods developed to study and diagnose the PEM fuel cells. These methods have been thoroughly reviewed by Wu et al. [3]. Among different techniques used the polarization curve, current interruption, cyclic voltammetry and electrochemical impedance spectroscopy are the most well-known electrochemical techniques in fuel cell studies. The polarization curve is the most common method of presenting and discussing the PEM fuel cells performance [1,3,4]. In this technique, the cell potential is plotted against the cell current (or current density) in various operating conditions. Usually, the plot is divided into three (or more) parts. It is believed that each part has a dominant performance loss. In the current interruption technique, the ohmic load is almost immediately released from the fuel cell and the voltage change is plotted vs. time. This method is often employed to investigate the ohmic losses in fuel cells [1,3]. In the cyclic voltammetry technique, the voltage increases linearly and sweeps back while the current is recording. The resultant voltage–current plot has peaks on potentials related to electrochemical reactions of the system [1,3]. Electrochemical impedance spectroscopy (EIS) is a well-established diagnostic and modeling method that has widely been used in electrochemistry [5–7] due to its flexibility (which enables covering a wide range of aspects of fuel cells) and accuracy.

In this paper, the studies conducted on PEM fuel cells using electrochemical impedance spectroscopy are reviewed. One of the most comprehensive reviews conducted in this field is the work published by Yuan et al. [4] in 2007. They discussed about various measurement and feeding modes in EIS as well as interpretation and EIS applications in optimization and contamination effects. This paper thoroughly reviews the recent efforts published in this field as well as aspects like Kramer–Kronig relations and process and measurement models, which were not covered in Ref. [4]. After introducing the EIS method and different aspects of the EIS technique (including the equivalent circuit and various defined elements based on electrochemistry reactions), the recent EIS applications are reviewed. The paper also highlights the novel studies performed and ideas developed based on the EIS method, and finally discusses common uncertainties and possible errors in the interpretation of the EIS measurements.

2. Electrochemical impedance spectroscopy

As mentioned before, the EIS technique performs based on imposing a harmonic perturbation to the system and measuring the impedance of the system in a wide range of frequencies. To measure the impedance in different frequencies, a frequency response analyzer (FRA) and a load bank are required. A sinusoidal wave is produced by FRA and applied to fuel cell via the load bank. Then, the system response is captured by FRA and an impedance spectrum is calculated [4]. The measurements can be conducted in the galvanostatic or potentiostatic modes, perturbing the current or voltage by the harmonic wave, respectively. It has been reported that there is no considerable differences between the galvanostatic and potentiostatic modes results [4]. However, the slope of the polarization curve is not significant in most of the performance domain, and hence a small perturbation in the voltage can cause a considerable change in the current, overloading the cell and the potentiostat circuits. Hence, the galvanostatic mode is usually preferred during impedance measurements [4]. The impedance measurement can also be conducted in both in-situ and ex-situ manners [4]. In the in-situ configuration, which has been widely used, the AC impedance of the fuel cell is measured as a whole; whereas, in the ex-situ measurement different components of the fuel cell are studied separately.

2.1. AC amplitude selection

One of the most important parameters in the AC impedance measurement is the AC amplitude. It is clear that the larger the AC amplitudes the easier the separation of the measured response from noises. However, the amplitude is limited due to the linearity assumption: in essence, the impedance is estimated by measuring the changes in the potential over the changes in the current. This calculation can be accepted if the potential changes linearly with respect to the current. Since this is not true for PEM fuel cells and other electrochemistry systems, the signal amplitude has to be small enough to satisfy the linearity assumption. Different studies [8–11] have indicated the AC signal amplitude equal to 5% of the DC performance current. For instance, the study conducted by Dale et al. [11] on the impedance spectra of a 2 kW stack for the selected AC amplitudes of 1%, 5%, 7.5%, 10% and 15% of the DC load shows that i) the spectrum is very scattered for low load currents, especially at a 1% AC signal amplitude for which it becomes difficult for FRA to distinguish between the response and noise; and ii) there is no considerable difference between the impedance plots in the amplitude range of 5%–10%.

2.2. Impedance plots

The Nyquist plot is the most usual way of presenting the impedance spectrum. In this graph, the imaginary part of the impedance (mostly presented with the negative sign) is plotted against the real part. The plot normally contains of two or more semicircles in different frequency ranges. Although the Nyquist plot is the most common representation in the EIS measurement technique, Bode magnitude (magnitude vs. frequency) and phase (phase vs. frequency) plots have also been used in the past [11–13] to extract information that cannot be readily obtained from the Nyquist plot. For instance, the local maximum values in the Bode phase plot show the characteristic frequencies which are proportional to the inverse of the time constants of the processes [13].

2.3. Wires impedance issue

The connecting wires can create significant magnetic fields affecting the impedance spectrum measurements [11]. This effect

can be controlled and minimized by i) spirally winding the connecting wires, ii) making perfect connections, and iii) using equal length coaxial cables to connect to FRA. The inductive effect of the wires on the impedance spectra at high and intermediate frequencies has been frequently reported in the past [11,14]. In fact, it has become a trend in the literature to interpret the positive inductive impedances at high frequencies as the inductive effects of wires. Attempts have also been made [15] in modeling this effect by resistor–inductor parallel connected elements in the equivalent circuit (see the next section) for high frequencies. Also, it is possible to use an open cell (as a calibration tool) to subtract the wires-related high frequency inductance effects from the measurements [16].

2.4. EIS weaknesses

The setup required for EIS measurement is expensive and the measurement time is considerably long [17]. The experiment is especially time consuming in low frequencies, and hence the uncertainty of the measurements is larger in this region [15]. The calculated parameters in the EIS models are only valid in the neighborhood of the tested point [17,18]. Also, it has been shown [19] that for cells with the active area larger than 25 cm^2, the currents are too high to be measured directly using standard electrochemical devices. Therefore, it must be calculated based on the voltage drop across a shunt that is placed in series with the fuel cell. However, the shunts are usually calibrated for DC currents and EIS AC perturbations can significantly affect their performance (due to skin effects and eddy currents) especially in high frequencies.

Moreover, the innovative experiment designed by Schneider et al. [20,21] shows that applying EIS AC harmonic perturbations to the fuel cell causes oxygen concentration oscillations in the gas diffusion layer which will be transferred to the air channel. This phenomenon especially occurs at frequencies less than 10 Hz. As a result, the low frequency arc in the Nyquist plot is affected and not easy to be interpreted. This effect has also been studied and verified by impedance models presented in Refs. [22,23].

Other weaknesses have also been claimed for which extensive studies in the field have shown to be not accurate. For instance the study of membrane dehydration using EIS has been questioned in past [24]; whereas other published results [25,26] have shown that EIS can be used for that matter.

3. Equivalent circuit

3.1. Process models vs. measurement models

The equivalent circuit modeling of fuel cells (and any other electrochemistry systems) can be classified in two categories: process models and measurement models. In the process models, the governing equations of the system are obtained and the electrochemical impedance is determined analytically. Then, the predicted impedance plot is compared with the measured impedances and the physical properties of the testing system are obtained. In the measurement models, on the other hand, the electrochemical impedance of the system is measured. An equivalent electrical circuit producing the same impedance plot is presented for interpreting different elements of the system.

Both process and measurement models have intrinsic problems and difficulties. For multipart systems such as fuel cells, the governing equations are very complex, and hence the process models are more complicated. Even if the electrochemical impedance of the system is determined analytically, it is not always possible to present an equivalent circuit that presents the calculated impedance graphically. Thus, it is difficult, if not impossible, to distinguish different resistor and capacitor elements in the fuel cell. Consequently, the physical descriptions of the system will be restricted. Moreover, because of considerable simplifications made in the governing equations, generally the predicted impedances are not in good agreement with the measured impedances. Due to these difficulties, the studies conducted based on the process models are limited in the literature [27–32]. Springer et al. [27] presented one of the most comprehensive studies on fuel cell modeling using the process model. The results are in good agreement with measured impedances; however, an equivalent circuit was not presented due to the complexity of resulting equations. The measurement models, on the other hand, are not presented clearly as functions of physicochemical properties and electrochemical reactions of the fuel cell. Thus, the physical meaning of the proposed elements is questionable. Although the elements of the proposed equivalent circuit can be determined based on measured impedances, these values are reliable only in the neighborhood of the calculated points and cannot be extended to the entire domain. Also, the correlations between physical properties and the equivalent circuit elements are not clear, and hence the physical properties cannot be extracted from the equivalent circuit. Finally, several electrical circuits can be presented to model a given impedance spectrum [5,18].

3.2. Randles model

The most common equivalent circuit used in the measurement models is the Randles circuit. This circuit, which is originally proposed by Randles [33,34], has been obtained based on the reaction of a metal ion in an aqueous solution using the process model.

The original Randles circuit includes a frequency-dependent resistor and capacitor, which are parallel to a conventional capacitor, and a conventional resistor which is in a series mode with the entire system. The Warburg element was introduced to the original circuit for the first time by Grahame [35]. He divided the electrochemical reactions in 6 different classes and presented various equivalent circuits. He presented the frequency-dependent characterizations of the resistor and capacitor which come from the linear diffusion equation in an anomalistic electrical element called Warburg. Fig. 1 shows the Randles circuit including the Warburg element. The Randles equivalent circuit has not been determined based on fuel cell governing equations. However, by replacing the conventional capacitor with another electrochemistry-based element, called constant phase element (CPE), this circuit can capture majority of impedance measurements of the PEM fuel cells as shown in the literature [25].

3.3. Other electrochemistry-based elements

There are modifications to the Randles equivalent circuit that can improve the predicted results. As mentioned above, the double layer capacitance can be modified to “constant phase element” (CPE) originated from non-uniform distribution of the current density along the electrode surface as a result of surface non-homogeneity [6]. Considering the capacitor impedance as $Z = 1/(C\omega j)$, where ω is the angular frequency and j is the imaginary unit, the impedance of a CPE element is defined as

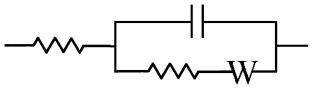

Fig. 1. Randles equivalent circuit.

$$Z_{CPE} = \frac{1}{Q(\omega j)^n} \quad (1)$$

where n is called CPE power and is due to physical properties. The CPE power is expected to remain constant during a wide range of operating conditions; otherwise it will be an extra degree of freedom (in the measurement models) reducing the difference between the fitted curve and the measured impedances [25].

Another modification is the implementation of the transmission line model (TLM) to study the catalyst layer as porous media [12,36–39]. The model has been presented to capture the variations of ionic resistances inside the electrodes [37,40], and assumes a network of cylindrical pores with uniform diameters in the catalyst layer [38]. In this method, the fuel cell (or a part of the cell) is modeled by a combination of electrical blocks. Each block contains normally a resistor–capacitor combination (Fig. 2). It has been claimed that this equivalent circuit represents the governing equations when the number of blocks approaches to infinity [39,41]. However, there is still debate regarding the consistency of the TLM with experimental results for low relative humidity [12].

In the electrochemistry literature, there is another electrochemical element for equivalent circuit that is called Gerischer element [42]. This element, which is a more general form of the Warburg element [32,43], appears when the diffusion (expressed by modified Fick's law [1]) and kinetic processes (expressed by the local-kinetic-related source term [32]) are coupled (e.g. coupling of electrochemical reactions with non-Faradaic diffusion in porous electrodes).

3.4. Kramer–Kronig relations

The impedance response of physical systems that satisfy causality (non-anticipativity), linearity and stability conditions has to obey the Kramer–Kronig relations [44]. In fact, Kramer–Kronig relations are mathematical relations that relate the real part of the impedance to the imaginary part. These relations can be employed to predict the imaginary part from the measured real part or vice versa. For the impedance response of the PEM fuel cell, the linearity condition can be satisfied by applying a perturbation with sufficiently small amplitude. The stability condition means that the system has to return to its original conditions after the perturbation is terminated. If the time constant of the tested processes is considerably higher than the measurement time period, it is assumed that the system is stable during the experiment. However, there are still concerns about the satisfaction of this condition in low frequencies which will be explained in the next section (Section 5.2) in detail.

It is proved [44] that electrical systems with passive (elements which cannot supply energy, e.g. resistors and capacitors) and distributed (e.g. transmission line models) elements satisfy the Kramer–Kronig relations. Thus, if the measured impedance is fitted to a presented equivalent circuit, it will satisfy the Kramer–Kronig relations [44]. However if it is not fitted properly, it cannot be concluded that the Kramer–Kronig relations are not satisfied. The poor fit can be because of employing insufficient equivalent circuit elements or inefficient regression methods.

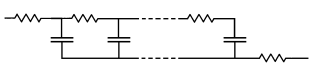

Fig. 2. Conventional transmission line model.

4. Applications of EIS and equivalent circuit

4.1. Temperature and humidity effects

There is a wide range of studies conducted on the effect of temperature, relative humidity and gas flow rates on the fuel cell performance. Aaron et al. [45] studied the effects of temperature, air-side humidity and air flow rate on the performance of fuel cells using the EIS technique. The experiments have been performed in the temperature range of 30 °C–50 °C, the humidity range of 20%–98% and the air stoichiometric ratios of 1.33–2.67. They also studied charge transfer resistance variations in different conditions. They concluded that the air-side flow rate does not affect the results considerably as long as it is maintained at stoichiometric ratios greater than 1.2. However, the reproducibility of their results is debatable. They stated that the response in the second measurements showed the same trend, but the values were approximately 8% larger than those obtained in the first measurement.

Malevich et al. [46] conducted research on the effect of relative humidity on the impedance plots, active area and charge transfer resistance. They compared the Nyquist plots of H_2/H_2, H_2/Air, H_2/O_2 and H_2/N_2 feedings and then presented the physical/chemical interpretations for various parts of the Nyquist plot. They reported that decreasing the relative humidity of reactant streams increases the membrane resistance and reduces the active area. They suggested that the change in charge transfer resistance of the cathode because of relative humidity is due to the change in the active area. Their research has been extended to the study of the effects of relative humidity on membrane and catalyst layer resistances and microporous layer influences [47]. They concluded that the presence of microporous layer in each of electrodes can have considerable effects on water management and humidity profile.

Danzer and Hofer [18] used EIS to study the dew point temperature in the humidifier, the excess ratio of hydrogen and oxygen and different operating points. They discussed about different equivalent circuits and found the equivalent circuit parameters via nonlinear least square method. They stated that the ohmic resistance in constant humidification was not affected by current densities. In essence, the increase in the relative humidity shifts the impedance plot solely toward lower ohmic resistances due to the increase in the water content of the membrane.

Brunetto et al. [48] studied different relative humidity and flow rates using EIS and found the optimum stoichiometric coefficients. They designed their own hardware and software to measure the impedance of the fuel cell and presented empirical correlations for the electrolyte resistance based on the impedance results. Their measurements and calculations indicated that among different stoichiometric (ST) ratios the ST values of 3 and 4, for hydrogen and air respectively, produce a relatively high performance with low reactant fluxes (which results in lower cost).

4.2. Sub-zero conditions

There are studies in the literature discussing about the fuel cell performance in sub-zero conditions. Hou et al. [49] measured the ionic resistance of the catalyst layer at four different current densities after eight freezing/thawing cycles. They reported that the catalyst layer ionic resistance decreases after cycles and the changes are not uniform. They studied the cold start process in sub-zero conditions in their subsequent paper [50] and concluded that the thin water film can cover pores among agglomerates and block the reactant gas. This topic was also studied by other research groups [51].

Mukundan et al. [52] studied the MEA effect in the PEM fuel cell performance at sub-zero condition. They reported that the rate of

voltage decrease in the sub-freezing environment is because of the increment of the charge transfer resistance. Furthermore, they found that MEA is the dominant factor in ice formation in the catalyst layer, and the ice formation is more close to the cell edges and flow field turns.

4.3. Catalyst layer

Nitta et al. [53] evaluated the contact resistance between the gas diffusion layer and catalyst layer as a function of the compression using EIS. They claimed that this resistance is a considerable part of the total ohmic resistance of MEA and can severely affect the current distribution inside the cell. They estimated this resistance from the intersection of the high frequency imaginary impedance in the Nyquist plot with the real axis which is the only extracted impedance data that they employed in their paper.

Eastcott and Easton [54] studied a catalyst layer without sulfonic acid groups. They used cyclic voltammetry and electrochemical impedance spectroscopy to investigate the effect of SiO_2 loading on catalyst layer conductivity and active area. They concluded that 45% SiO_2 loading maximizes the active area although the fuel cell performance was lower than that achieved with Nafion-based catalyst layers. In their subsequent paper [55], they studied the ceramic carbon electrodes and claimed it has similar performance to Nafion-based electrodes.

Seo et al. [56] estimated the interfacial resistance between the membrane and catalyst layer by feeding H_2/H_2 to the fuel cell and then measuring the frequency-dependent impedance. Their presented equivalent circuit is an arbitrary measurement model which can be employed to model the measured impedances; however this model is not based on any physical/chemical analysis and hence the presented conclusions from the impedance measurements have not been verified. Cimenti et al. [12] used EIS to measure the catalyst layer proton resistance using H_2/N_2 and H_2/O_2 feeding methods. They modeled the catalyst layer with a transmission line model (TLM) and employed ZView software to fit the model to the measured impedances. They stated that TLM does not produce a good fit for dry conditions. They also found that the H_2/N_2 feeding method is capable of measuring the catalyst layer resistance at equilibrium and extracting micro-structural information. This method is also preferred due to its low measuring time and simple data analysis. They also used this method to study the catalyst layer resistance dependency to relative humidity and concluded that decreasing the relative humidity increases the catalyst layer resistance in an almost exponential trend.

Manzo et al. [57] studied the cathode catalyst layer and presented a process model based on diffusion and current generation equations. Using the equivalent circuit proposed in Refs. [58], the anode and contact impedances were separated from the fuel cell impedance plot and the cathode impedance was compared to the simulated results generated based on the governing equations. This separation of the fuel cell impedances into anode, cathode and contact impedances is based on the assumption that the origin of the high frequency semicircle in the Nyquist plot is from the anode impedance. However, this assumption has been questioned in literature [4]. Using the same methodology, the same group studied the low-current electrochemical mechanisms of the fuel cell separately [59] based on the assumption that mass transport limitations are negligible in low current densities. In both of their papers [57,59] the theoretical formulations were transferred to the time domain, and spatial and temporal current distributions were calculated and discussed.

There is a group of published studies in literature regarding the catalyst layer studies which employed EIS besides other experimental methods such as polarization curves, cyclic voltammetry (CV), transmission electron microscopy (TEM), scanning electron microscopy (SEM), X-ray diffraction (XRD) and N_2 adsorption–desorption [60–69]. In all of these studies, the EIS is used to verify the results obtained from other methods rather than specifically discussing the measured impedances. Moreover, these studies often used simplifications in their EIS theory and hence their discussions and the conclusions based on their assumptions are often questioned in literature [4,5].

4.4. Gas diffusion and microporous layers

The EIS technique has also been used to study the effect of the gas diffusion layer on the cell performance. Bultel et al. [70] studied the effect of slow oxygen diffusion in the gas diffusion layer on the fuel cell behavior at various cell temperatures and relative humidities. Using different inert gases under the depleted oxidant concentration condition, they concluded that oxygen diffusion is the major concern and the oxygen diffusion coefficient in the gas diffusion layer is a governing parameter affecting the fuel cell performance regardless of the oxygen concentration. In the recent work conducted by Maidhily et al. [71] the GDL has been studied by measuring the impedances of the cathode and anode separately using H_2/H_2 and air/air feedings. Physical interpretations about different elements in the equivalent circuit were presented. However, the reported physical and chemical interpretations can be questioned due to the simplified assumptions employed. Another study conducted on the GDL using EIS is the work of Dotelli et al. [72] who used the combination of the polarization curves and impedance measurements to clarify the role of the GDL. In their study, where three different GDLs were used, five different impedance measurements have been obtained in each tested current densities, and the average values were presented as the final impedance spectra. They reported that the main difference between the tested GDLs is their contact resistances. They also confirmed that the presence of microporous layer (MPL) improves the performance of the GDL, especially at high current densities mainly due to decreasing the contact resistance. They also claimed that increasing the compression reduces the fuel cell performance at high current densities.

Omati et al. [73] studied four different GDLs and their role in the fuel cell performance using both polarization curves and EIS. They presented a simple equivalent circuit and calculated different resistances based on the circuit. They reported that the GDL with the smallest thickness and weight produces the best performance. The same research group prepared a multi-wall carbon-nanotube-based gas diffusion medium and tested it using the fuel cell performance measurements and impedance characteristics [74]. Similar equivalent circuit was used. They found that adding carbon nanotubes increases the fuel cell performance. In their proposed equivalent circuit, the cell impedance has been divided into two parts showing the effect of the charge and mass transfer limitations; however, this conclusion has not been completely proved in literature.

The effects of the MPL on the performance and impedance behavior of the fuel cell have also been studied by Malevich et al. [58]. The ohmic, charge and mass transfer resistances at different current densities were extracted from the impedance plots. They reported that the MPL decreases the mass transfer resistance without changing the charge transfer resistance, decreases the through-plane gas permeability of the porous layer, reduces water saturation in the porous layer, improves oxygen transport to the cathode catalyst layer and consequently increases the fuel cell performance. In their subsequent paper [36], the same research group measured the catalyst layer resistance and effective protonic conductivity by feeding H_2/N_2. They found that the assumption of

homogenous catalyst layer structure as well as modeling the catalyst layer with the uniform resistance and capacitance in the equivalent circuit are not accurate. They employed transmission line models to capture the catalyst layer non-homogeneities which can be due to relative humidity in the measurement [37], the catalyst layer preparation method [37] and the level of ionomer impregnation in the catalyst layer [75].

Other studies on the effect of the GDL and MPL using EIS [76–80] have been based on arbitrary equivalent circuits. These circuits have been used to model the impedance plots and to explain the physicochemical properties. However, the presented equivalent circuits must be recognized as measurement models which can only be used to compare the impedances in different conditions and no physicochemical interpretation and conclusions can be presented based on the element values.

4.5. Membrane

The EIS technique has also been used to study the ionic conductivity of the membrane. Membrane ionic conductivity measurement using two-probe and four-probe techniques was compared by Mikhailenko et al. [81]. In two-probe technique, the response of the system is measured via the same electrodes to which the perturbation is applied. In the four-probe technique, on the other hand, measuring the system response and applying the perturbation to the system are achieved via two different pairs of electrodes [82]. They concluded that two-probe technique is less complicated, has simpler geometry, and is less prone to the experimental errors. Also it has been shown that the cell geometry and electrode arrangement has considerable effects on frequency dependent response. The ionic conductivity measurement has also been discussed by other groups [83] and it was shown that the ionic conductivity of their experimental membrane is similar to Nafion.

Soboleva et al. [16] determined the conductivity of various Nafion membranes by measuring the impedances in two perpendicular directions. To eliminate the inductive effects of the connecting wires in high frequencies, the impedance of the 'opened cell' was measured and subtracted from the subsequent measurements. The typical Nyquist plot of a membrane is shown in Fig. 3. To extract the through-plane membrane resistance from the Nyquist plot, two different methods in the literature are employed [16]. In the first method, the resistance is determined by extrapolating the linear portion of the low frequency part of the Nyquist plot to the real part axis (x-axis). This point is assumed to be the through-plane resistance. In the second method that seems to be more accurate, however, the high frequency part of the impedance is modeled with a parallel combination of a resistor and a capacitor. The resistance is assumed to be the through-plane membrane resistance. Soboleva et al. [16] calculated the resistance via both methods and concluded that the deviations are less than 10%.

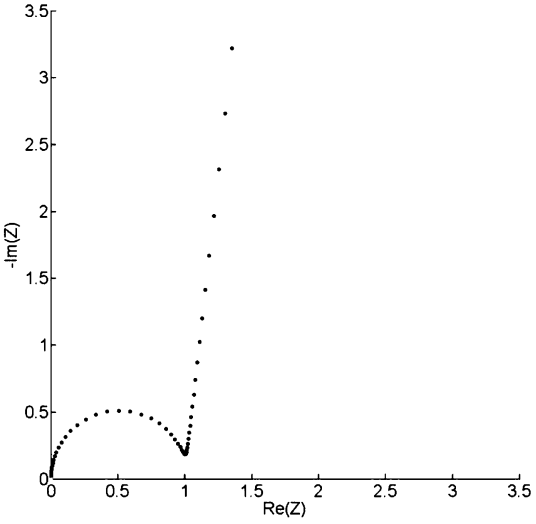

Fig. 3. The typical Nyquist plot of a membrane.

Liu et al. [39,84] employed EIS to quantify the through-plane RH-dependent membrane resistance for various ionomer/carbon weight ratios and various operating conditions using H_2/N_2 feeding. They reported that the proton conductivity in tested electrodes starts to drop when the ionomer volume fraction becomes smaller than 13%. A transmission line model was developed to represent the governing equations [85]. Jang et al. [37] have presented a complex capacitance analysis for estimating the catalyst/ionomer interfacial capacitance and ionic resistance. They concluded that the resistance is higher for MEAs with lower ionomer content.

Legros et al. [24] employed ex-situ EIS and acoustic emission methods to estimate the water amount in the membrane. In the acoustic emission method, the sample is exposed to a produced wave and the elastic energy of the sample is determined by measuring sample surface displacement with piezoelectric sensors attached to the sample surface. Based on the data, they reported that the acoustic emission technique is more sensitive to drying processes than EIS. Huth et al. [13] estimated the proton transport of the membrane of a high temperature PEM fuel cell by feeding the pure nitrogen to the cathode and measuring the impedance. They presented the fuel cell Bode diagrams at different pressures and temperatures. They claimed that the proton transport is the limiting process when there is enough hydrogen supply at the anode. Navarro et al. [86] used a pore-filling electrolyte membrane fabricated based on plasma-activated microporous polyethylene matrices to study the performance of the fuel cell. They employed EIS to measure the electrical response. They reported the Nyquist plots of single cells; while feeding both electrodes with hydrogen and oxygen. In their results the impedances of the connecting wires are dominant, especially in hydrogen feeding plots. Tsampas et al. [87,88] studied the proton transport mechanisms in the fuel cell membrane using EIS. They claimed there are two different mechanisms for proton conduction in the fully hydrated Nafion membranes: proton migration in the aqueous and proton transfer between adjacent sulfonate groups in narrow pores. They stated that at low hydrogen partial pressures, the dominant proton transport mechanism is the second one which is the reason of the steady-state bistability performances (i.e., two different potential values corresponding to the same current density) in the fuel cells. They reported negative real part impedances with large imaginary components in the Nyquist plots for these performance conditions. Considering the fact that the real part of the impedance values in low frequencies are the negative of the slope of the polarization curves and the polarization curve has positive slope in the bistability points, it is reasonable to have negative real parts in the Nyquist plot. These negative real parts have also been reported before in metal corrosion [89,90] and direct methanol fuel cells [91]. Furthermore they stated that the proton transport time constant can be as large as 10 s, and hence it can be the limiting process in the fuel cell.

Lamy et al. [92] reviewed the effects of the electrochemical characteristics of the membrane on the fuel cell performance. They simulated the mass and charge transport inside the membrane and then theoretically studied the influence of the catalyst layer and GDL porosity on impedance diagrams. As part of their study, they optimized the operating parameters which resulted in the fabrication of their new membrane electrode assembly.

Finally, it has to be reemphasized that there are other studies on the membrane which employed EIS besides other methods, like X-ray diffraction, transmission electron microscopy, scanning electron microscopy and cycle voltammetry. In these works, the EIS results are only used to verify measurements of the other methods [93–95].

4.6. Contamination

The use of EIS in studying contamination of electrodes have been summarized by Yuan et al. [4] who have thoroughly reviewed the effects of CO, NH_3 and H_2S contaminants on the fuel cell. Li et al. [96] used EIS to study the effects of relative humidity, Pt loading, and toluene contaminations on the air side electrode. They reported that the contamination effects were amplified by increasing the current density, increasing the toluene concentration, decreasing the relative humidity, and decreasing the cathode-side Pt loading. Furthermore, they concluded that the contaminants have long-term effects on the fuel cell performance which cannot be fully recovered. They added the effect of the chloride contamination in their following study [97] and found out that because of chloride contamination, the cell voltage tolerates an initial sudden drop followed by a plateau. Martinez-Rodriguez et al. [98] also studied the effect of chlorinated impurities on the fuel cell performance. They reported that even 0.05 ppm impurity decreases the cell performance rapidly for the voltage range above 0.2 V below which poisoning has no effect. Nakajima et al. [99] studied the effects of CO poisoning on polarization curves and impedance plots. They fed the anode with a mixture of CO and H_2 and conducted anode impedances and I–V measurements. They reported that that the output voltage depends on CO poisoning.

The nonlinear frequency response analyzer (NFRA) has been used to diagnose simultaneously the processes of membrane dehydration, fuel cell flooding and anode CO poisoning [100]. This method, which applies high amplitude sinusoidal perturbations to the system and measures the response, is highly sensitive to distinguish between phenomena having approximately the same time constants. For instance, the CO poisoning and dehydration cannot be distinguished from the EIS results; whereas, they are totally distinct in NFRA. Kadyk et al. [101] studied the anodic CO poisoning in a symmetrical H_2 feeding cell by polarization curves, EIS and NFRA. They used a theoretical model from the literature and simulated the NFRA results. The experimental measurements and simulated results were in good agreement. They also employed the H_2/H_2 feeding system to study the spectra related to the beginning of CO poisoning in anode during fuel cell operation and reported an additional arc in Bode plot in low frequencies at 100 ppm.

Andreasen et al. [15] studied the effect of operating temperature, current density and CO and CO_2 contaminants in the anode input gas on the performance of the high temperature PEM fuel cells. They reported that the contaminants affect the entire range of frequency spectra. The results showed that the high frequency part of the Nyquist plot was affected mostly by poisoning. They repeated every measurement two times and presented the RMS values. They declared that the discrepancies between most measurement pairs were less than 2%. It is necessary to reemphasize that there is no clear connection between fuel cell governing equations and measurement models and hence the physicochemical interpretations of the presented equivalent circuits need to be reinvestigated [96,99,102].

4.7. Aging and durability

Roy et al. [103] studied the membrane aging by different physical and electrochemical techniques including EIS. They reported that the low-frequency inductive features are related to phenomenon on aging. They also reported that high frequency part of the impedance is dependent to the electrochemically active surface area. Nara et al. [104] studied the degradation of the cathode catalyst layer using EIS, transmission electron microscopy, field emission scanning electron microscopy, cyclic voltammetry, micro-Fourier transform infrared spectroscopy and nitrogen adsorption–desorption measurements. They presented a new transmission line model as the equivalent circuit for the cathode catalyst layer considering the distribution of the oxygen reduction reaction in pores inside and outside the agglomerates (primary and secondary pores). The presented model agrees well with the measured impedances; however, this agreement can be the result of the high number of elements used in the proposed equivalent circuit which causes high degrees of freedom of the circuit.

Fouquet et al. [25] reported the state-of-health of a PEM fuel cell in a qualitative manner. They considered the state-of-health of the fuel cell based on the dehydration and flooding conditions. However, the state-of-health has to be defined in a more general manner to cover other aspects of fuel cell performance (poisoning, aging, etc.). There are also other studies on aging and degradation using EIS. However, these studies do not present a clear connection between the elements of the measurement-model-based equivalent circuits and the physical and chemical properties of fuel cell [105–110].

4.8. Dehydration and flooding

The EIS technique has also been used to study flooding and dehydration in the fuel cell. One of the examples is the work of Fouquet et al. [25] who reported that flooding and dehydration in the PEM fuel cell cannot be distinguished from the polarization curves. They modified the Randles classic equivalent circuit by changing the double layer capacitance with a constant phase element (CPE) and found the best fit between the model and the measured impedances. They assumed the power in the definition of CPE to be constant to have a physical meaning and avoid an additional degree-of-freedom in data fitting algorithms. Based on the proposed equivalent circuit, they measured the membrane polarization and diffusion resistances and defined three subspaces that are related to nominal, flooded and dry conditions. These subspaces can be used to predict the flooding and dehydration conditions from the impedance measurements.

Bautista et al. [31] presented a process model to predict the impedance response and polarization curve of the PEM fuel cell. They considered reactant and products mass transfer in the channels and water transport across the membrane. Using the simulated Nyquist plot, they studied the effect of dew point temperature (humidity), the membrane thickness, cathode gas backing porosity and the agglomerate thickness. They were able to distinguish between flooding and dehydration effects employing impedance responses.

Kurz et al. [26] used EIS to diagnose the flooding and dehydration phenomena. From the results, they concluded that the measurement of the imaginary part of the impedance at 0.5 Hz and real part of the impedance at 1 kHz will be sufficient to distinguish between flooding and dehydration. They called these two points “Flooding Indication Value” and “High Frequency Resistance” respectively. Measuring these two impedances they predicted flooding and drying nearly half an hour prior to the time required to be observed in the polarization curves. Based on the diagnosis, they presented an equation and a control parameter that can adapt the air flow rate of the tested fuel cell stack to prevent flooding and drying. The presented control algorithm can be modified for

various operating conditions, temperatures, current densities and relative humidities.

Roy and Orazem [111] reported that flooding can be predicted based on the standard deviations of the measured impedances. They stated that the formation and removal of water droplets are stochastic processes, and hence, can be predicted by a technique oriented toward deviation measurements. They claimed that the cell impedance and impedance measurement deviations increase considerably during flooding. This increment is more at the real part of the impedance and low frequencies which is close to the flooding characteristic frequency. In their next study [112], they presented a graphical method (estimating the parameters graphically) to determine the constant phase element (CPE) coefficients in high frequencies. They stated that decreasing this capacitance is a sign of flooding and drying as well. They measured the impedances at different current densities, times, temperatures, back pressures, flow channels and gas diffusion layers.

Schneider et al. [113] studied the impedance responses of the dehydrated and fully humidified Nafion membrane using EIS and current step measurements. They reported that the low frequency inductive loop in the Nyquist plot is due to the change in conductivity of the dehydrated membrane and slow uptake and release of water in the low-humidity membrane. They reported that the time constant of the membrane hydration by-product water is around 25 s.

Rodat et al. [114] studied flooding and drying of a fuel cell stack and individual cells by EIS in various operating conditions. However, there are some concerns about their frequency range and equivalent circuit. The considered frequency range (3 Hz–5 kHz) cannot cover all the phenomena in the fuel cell. Kadyk et al. [100] distinguished flooding, membrane dehydration and CO poisoning simultaneously using nonlinear frequency response analysis (NFRA) and concluded that the dehydration and flooding could be diagnosed clearly from linear response analysis (EIS).

4.9. Other phenomena diagnosed by EIS

There are other studies in which other aspects and elements of fuel cells have been monitored using EIS. These examples include the structure of the flow channels, mass transport in the cathode side, clamping effect and the stack performance. For instance, Kwon et al. [115] studied three different serpentine channels using EIS. The channels were modeled by computational fluid dynamics methods and then the resistances were compared by impedance measurements. They reported that their EIS-based conclusions are in good agreement with their previous experimental and modeling results.

Using a process model, Mainka et al. [28] analyzed the mass transfer in the cathode of the PEM fuel cell. They claimed that the limiting layer for mass transport is the active layer, and the mass transport resistance of the GDL in a normal condition is negligible. They proposed that the Warburg element has to be in series with the membrane resistance and the only parallel elements have to be the double layer capacitance and charge transfer resistance. In their next papers [29,116], they discussed about the accuracy of the constant oxygen concentration assumption at the gas channel/GDL interface. They considered the gas consumption along the channel which enabled them to capture the local variations of impedance spectra and diffusion kinetics.

Asghari et al. [117] studied the effect of the clamping torque (in terms of magnitude and non-uniformity) and the operating temperature on the fuel cell performance and break-in procedure (referred to as a condition providing enough hydration in the membrane and electrodes before the peak performance point) using EIS. They claimed that non-uniformity of clamping torque has inductive characteristics at high frequencies and can increase the ohmic resistances observed in Nyquist plots. They stated that the inductive effects may be due to non-uniform current distribution especially within the GDL. They presented the optimum clamping torque based on the variations observed in different resistances. Furthermore, they claimed that increasing the operating temperature decreases the charge transfer resistance and also the EIS method can be employed to monitor the break-in process.

The impedance measurement has also been conducted on the fuel cell stacks or one special single cell in the stack [e.g. Refs. [11,14,19,26,48,118]]. There are remarkable studies on the fuel cell stack accessories or the effect of the cell position [11]. For instance, the work of Dale et al. [11] shows that the ohmic resistance is dependent to the cell location and the lowest ohmic resistance observed for the closest cell to the air inlet. They have also measured the capacitor or inductor effects at high frequencies and showed that the inductor effects occur for cells close to the hydrogen inlet. Finally, various accelerated conditioning methods for PEM fuel cells using different experimental techniques including EIS were compared by Yuan et al. [119].

5. Outstanding ideas

There are novel ideas in the literature related to interpretation and measurement of the impedance results of fuel cells. They are elaborated in this section.

5.1. EIS interpretation

Malevich et al. [46] measured the impedance spectra of a fuel cell for H_2/air, H_2/O_2 and H_2/H_2 feedings. They indicated three different semicircles in the H_2/air Nyquist plot at high (60–0.6 kHz), medium (600–3 Hz) and low (3–0.1 Hz) frequency ranges and called them HF, MF and LF, respectively. They stated that LF arc is diminished when pure oxygen is employed. As a result, they concluded that the LF arc originates from impedance characteristics of the processes related to mass transport such as oxygen transport. Their results showed that i) the increase in the current density reduces the size of the MF arc; ii) the charge transfer resistance is inversely dependent to the current density; and iii) the MF arc in the H_2/H_2 feeding does not appear. Based on these conclusions they stated that the MF part of the Nyquist plot is related to the cathode charge-transfer resistance. The HF arc is seen in all the feedings and is the only arc observed in the H_2/H_2 feeding. Based on the hydrogen evolution reaction (hydrogen gas production by the reduction of hydrogen ions), hydrogen oxidation reaction in the H_2/H_2 feeding setup, and hydrogen oxidation reaction in H_2/O_2 and H_2/air feeding setups, it can be concluded that the HF part is related to the hydrogen oxidation reaction. However, they have discussed about the inappropriateness of this conclusion. The result from experiments in different relative humidity has shown that the diameter of the HF arc (equivalent resistance value) is in fact dependent to the protonic resistance of the membrane and catalyst layers.

5.2. EIS measuring methods

Brunetto et al. [48] investigated the AC perturbation amplitudes in EIS measuring. They claimed that the response of the differential governing equations of the fuel cell can be assumed linear if the AC perturbation amplitude is smaller than so-called thermal voltage, V_T, defined as

$$V_T = RT/F \tag{2}$$

where R, T and F are the gas constant, cell absolute temperature and Faraday constant respectively. Considering the cell temperature of

80 °C, the thermal voltage can be calculated as 30 mV. It means that the AC perturbation amplitude for the PEM fuel cell in the EIS measuring process has to remain equal or less than 30 mV. This concept has also been presented and discussed before [120].

Roy and Orazem [121] applied the consistency evaluation methodology proposed by Agarwal and Orazem [44] to the fuel cell impedance data. They used the Kramer–Kronig relations to predict the imaginary part of the fuel cell impedance response based on the measured real part. By comparing the predicted imaginary part with the measured imaginary part they found the points outside of the confidence interval. This method can be employed to determine the measurement points which are not consistent with the Kramer–Kronig relations. In their measurements, the impedances measured at frequencies higher than 1000 Hz and lower than 0.05 Hz were inconsistent with the Kramer–Kronig relations. They showed that the low-frequency inductive loops in the fuel cell impedance plots are self consistent and hence, are related to the physics of the fuel cell.

Brunetto et al. [48] introduced a new perturbing method called Multi-sine method. In this method, instead of applying a simple sinusoidal waveform to the system, some harmonics are added to the perturbation signal. The comparison between the normal and Multi-sine techniques shows that there is only a slight difference in the low frequency region. The measuring time of the Multi-sine technique is less, and it minimizes the system perturbation. In their experiments, the measurement of the impedance spectra by the normal technique takes 16 min; whereas, it takes less than 5 min by the proposed Multi-sine technique. As a result, the Multi-sine technique can be more suitable, especially for diagnostic applications (e.g. dehydration or flooding in fuel cell stacks).

Kadyk et al. [100] applied the method called the Nonlinear Frequency Response Analysis (NFRA) to study simultaneously different aspects of the fuel cell. As mentioned before, in the electrochemical impedance spectroscopy technique, a sufficiently small stimulated signal is applied to the system and the response is measured. To find the impedance in EIS, the derivation of the potential with respect to the current is replaced by the potential change to the current change ratio. Therefore, the signal has to be small enough to satisfy the linearity assumption. However, in the NFRA technique, a high amplitude signal is applied to the system which results in introducing a nonlinear distortion to the response. It has been shown [100] that the first term in NFRA is the linear system response that is equal to the classical EIS response. Kadyk et al. [100] also employed the second order response and investigated the membrane dehydration, flooding and anode catalyst poisoning in the fuel cell simultaneously. Instead of measuring the system response to a harmonic noise, Jung et al. [122] applied an iterative step change to the resistive load and measured the fuel cell response. They presented a mathematical approach to find the values of their equivalent circuit elements.

Schneider et al. [113] studied the fully humidified and dehydrated Nafion membrane impedances by EIS and current step tests. In both tests, a sinusoidal high frequency current was superimposed to the applied current. Then, the high and low frequency responses were independently separated and studied using analog filtering. The high frequency response was employed to estimate the ionic resistance of the membrane.

5.3. Innovative hardware

An innovative, cost effective impedance measurement setup has been introduced by Brunetto et al. [48]. The desired AC perturbation is created in a function generator and then superimposed to the working DC current in the electronic load part. Then, the current is applied to the fuel cell and voltage is measured. The acquired voltage and current wave forms are transferred to a personal computer (via General Purpose Interface Bus link (GPIB)), which are then converted to the frequency domain by a Fast Fourier Transform (FFT). The impedance spectra can be determined by simply dividing the voltage to the current. LabVIEW™ has been used to control the entire process.

Wasterlain et al. [123] presented a new PEM fuel cell impedance measurement device, which is capable of simultaneous measurement of 31 modules, and compared the measured impedances with other impedance meters. They identified the acceptable accuracy of the device and claimed that the equipment cost is nearly half of other commercial devices.

Bergmann et al. [124] presented a new apparatus capable of measuring the impedance and temperature distribution of various segments of a high temperature PEM fuel cell. The apparatus is made of 50 synchronized potentiostats and channel Frequency Response Analyzers (FRA) facilitating the measurement of the current, voltage and cell impedances in 50 different segments of the tested fuel cell in both potentiostatic and galvanostatic modes for a frequency range of 0.1 mHz–20 kHz. Each segment covers an active area around 0.5 cm^2. The generated exciting perturbation is synchronized by hardware to reduce the interaction of adjacent cell segments during EIS measurements. The system can be setup for higher accuracy or faster measurements. The connecting wires were chosen from extremely low-inductive cables to minimize the noise. Furthermore the temperature distribution of the cell can also be measured in the presented setting. They concluded from their results that the overall impedance measurements cannot capture the lateral inhomogeneities of fuel cells, and hence it cannot present a complete picture of the governing processes.

Soboleva et al. [16] presented two different experimental facilities to measure the in-plane and through-plane conductivity and impedance of the membranes separately. They discussed about required calibrations and errors during measuring process.

5.4. Other innovative ideas implemented using EIS

Dale et al. [11] stated that the fuel cell stack is generally controlled by an embedded control board in real applications. Thus, the control processes, such as purging, have to be considered in impedance studies and other methods. In the purging process, the hydrogen purge valve at the stack is opened at regular intervals to flush out of the cell the migrated nitrogen and produced water to the anode. They used a control system to control purging based on the cell voltage drop which occurs due to nitrogen crossover and flooding in the anode.

Danzer and Hofer [17] presented a new method called Electrochemical Parameter Identification (EPI) to study the PEM fuel cells (and other electrochemistry systems). Unlike the EIS, the EPI method strictly works in time domain: while the measured impedances are transferred via Laplace or Fourier transformations to the frequency domain in the EIS method, the EPI method models the impedances in the time domain and determines the proposed equivalent circuit elements values directly from the current and voltage measurements. In their method, the voltage is measured as the current is applied. An optimization algorithm was used to calculate the values of the equivalent circuit elements. Like EIS, these values are only valid in the neighborhood of the measuring point. Moreover, the parameters obtained using EPI is less accurate than those obtained using EIS. However, the EPI measurement time (1–5 s) is considerably shorter than EIS measurement time (3–10 min). Also, the EPI method is less expensive to implement as it does not require a frequency analyzer.

Rubio et al. [125] considered a simple equivalent circuit to model the fuel cell. They transformed the equivalent circuit

impedance response to the Laplace domain and simplified it to a second order fractional term and then determined the constants of the model. The methodology is based on the assumption that the relevant cell phenomena (such as charge transfer) occur in the frequency range of 1 Hz–5 kHz. The experimental apparatus required in this method are inexpensive and portable. This method has been used [126] to study flooding, drying and carbon monoxide poisoning effects on the fuel cell performance.

Deseure [127] combined the Continuous Stirred Tank Reactors (CSTR) approach with EIS to model the fuel cell. The CSTR approach was used to model the gas transport in the channels. In this method, the channel is divided into fine elements and each element is supposed to be an ideal reactor with perfect mixing [128]. The mass balance in the gas channel was modeled by a series of CSTRs. The electrode was divided into successive parts each of which was in contact with a single CSTR. It was supposed that the gas transport is infinitely fast, and hence the gas composition for each CSTR is homogenous. As a result, it was possible to model the fuel cell based on the process model and present the calculated Nyquist plots. In this work, the predictions have not been verified by experimental results. There are also inconsistencies between the presented Nyquist plot and typical measured Nyquist plots presented for PEM fuel cells in the past [e.g. Ref. [46]].

O'Rourke et al. [129] presented a method to estimate the cathode flow rate using impedance measurements. They stated that the anode flow rate does not have considerable effects on the impedance spectrum. The cathode flow rate, on the other hand, can be estimated from the AC magnitude at 0.1 Hz even at current densities as low as 0.1 A cm^{-2}. They presented an algebraic equation to predict the cathode flow rate in the PEM fuel cell from 0.1 Hz impedance magnitude. They claimed that the accuracy of the predicted flow rate from impedance measurement is in the range of flow meter accuracy.

Pattamarat and Hunsom [130] employed 2^k factorial design and estimated the effects of the cell voltage, flow rates and cell temperature on the fuel cell performance. Then, using ANOVA techniques, they estimated the interactions of different factors and their effects on the performance. A simple equivalent circuit was used to model the cell outputs. The circuit was based on a measurement model. Thus, the physical interpretations of the circuit elements are questionable.

6. Debates in the literature

6.1. Uncertainties in measurement models

As stated before, the EIS models can be divided into the process models and measurement models. Most studies are based on measurement models. However, the parameters in these models are not directly related to physicochemical properties of the fuel cell [18]. Although there are some indications about the involved processes in high, intermediate and low frequencies in the impedance plot, even the governing parameters of these processes cannot be correlated to the values of the equivalent circuit elements in the measurement models. As a result, the physical and electrochemical parameters of the fuel cell cannot be quantified based on the measurement models. Also, there are doubts about the processes involved in different frequencies ranges [46]. Moreover, because the measurement-model-based equivalent circuits are not directly related to the physicochemical properties of the fuel cell, the fitted values and even circuit elements are validated just in the neighborhood of the tested point. It means there is no guarantee that the values of the parameter or equivalent circuits are applicable in other current densities, operating temperatures, and hydrogen and air flow rates [17,18].

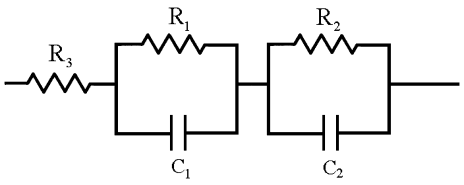

Fig. 4. Proposed electrical circuit.

Several equivalent electrical circuits can be established to model a given impedance spectrum [5] and hence based on different studies and research goals, various versions of equivalent circuits have been presented in the literature. Consequently it is impossible to combine different interpretations and describe the physical meaning of various elements of the circuit. It seems that a 'standard' equivalent circuit based on a process model is needed to lead the EIS-based studies of the fuel cell toward physical and electrochemical interpretations of circuit elements. Nevertheless, there are remarkable qualitative conclusions from impedance spectrum studies using measurement models [e.g. Ref. [46]].

6.2. Frequency range

There have been debates regarding the frequency range and related interpretations in the EIS measuring and modeling. It has to be mentioned that if the time constant of a process, τ, is small enough to satisfy the condition of $\omega_{max}\,\tau << 1$ this process cannot be captured by the Nyquist plot [16].

Another issue is about the importance of low frequency impedances. Fig. 4 shows a simple electrical circuit that will be used for the following discussion. Fig. 5 shows the Nyquist plot obtained for $R_1 = R_2 = R_3 = 1\ \Omega$, $C_1 = 0.01$ F, $C_2 = 0.1$ F and the frequency range of 10 mHz–100 kHz (which is a common range in the EIS measurement of the fuel cell [4]) with 100 points. The plot has two peaks: the one on the right hand side is related to low frequencies and that in the left hand side is determined by high frequencies. It is known that the parallel combination of a resistor and a capacitor produces a semicircle in the Nyquist plot [131]. Thus, the peaks in the Nyquist plot are in fact the summits of semicircles that convoluted in each other. The graph starts from 1 Ω at high frequencies as the R_3 resistor moves the graph to the high Re(Z) values. The resistor values (R_1 and R_2) in the R–C parallel combination blocks define the semicircle diameter and the capacitor moves the semicircle in the frequency range. In this example, $R_1 = R_2 = 1\ \Omega$ and hence the total range of the two convoluted semicircles is 2 Ω.

The Nyquist plot of the proposed circuit with $R_1 = R_3 = 1\ \Omega$, $C_1 = 0.01$ F, $C_2 = 0.1$ F and $R_2 = 10\ \Omega$ is presented in Fig. 6. The low frequency semicircle diameter is increased to 10 Ω and it is totally

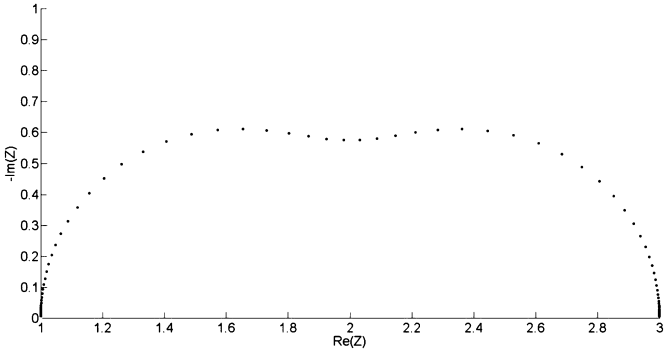

Fig. 5. Nyquist plot of $R_1 = R_2 = R_3 = 1\ \Omega$, $C_1 = 0.01$ F and $C_2 = 0.1$ F.

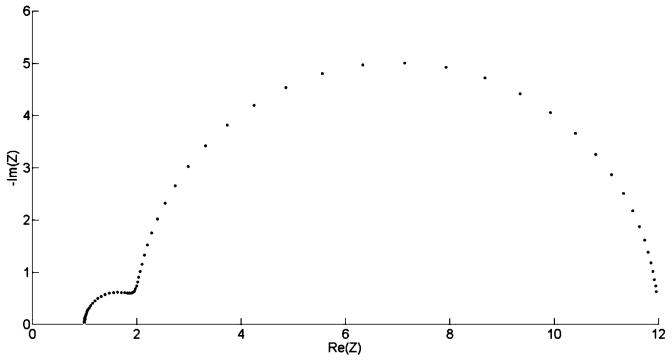

Fig. 6. Nyquist plot of $R_1 = R_3 = 1\ \Omega$, $C_1 = 0.01$ F, $C_2 = 0.1$ F and $R_2 = 10\ \Omega$.

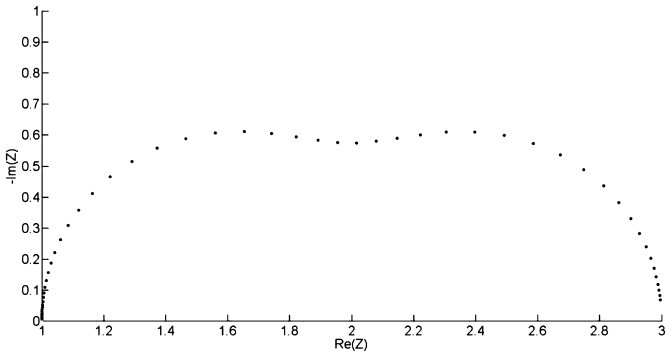

Fig. 8. Nyquist plot circuit with $R_1 = R_2 = R_3 = 1\ \Omega$, $C_1 = 1$ F, $C_2 = 10$ F and frequency range of 1 mHz–100 kHz.

distinguishable from high frequency semicircle with 1 Ω diameter. It clears that the low frequency semicircle is related to the higher capacitance ($C_2 = 0.1$ F), and hence low frequency ranges of the Nyquist plot are affected by higher capacitances. The measured impedances in low frequencies provide useful information although its uncertainty is higher due to longer measuring time [15]. Furthermore, considering the time constant definition of a parallel resistor–capacitor combination as $t = RC$, the higher capacitances are equivalent to larger time constants, and hence slower reactions. Since the most important and controlling reactions of the fuel cell are the slowest reactions, one can conclude that the low frequencies in the Nyquist plot are the most important part of the plot. Although the measurement in the low frequencies are in a way that the system is changing gradually during acquisition [132], the frequency range cannot be restricted to higher levels and the experimental setup needs to be modified in a way that the low frequencies can be captured in a quasi-stable condition. Since in very low frequencies (DC mode) the Nyquist plot does not have the imaginary part, a closed semicircle in this range ensures covering the acceptable frequency range.

6.3. Nyquist plot adequacy

There are also concerns about the adequacy of the Nyquist plot consistency with experimental results. Fig. 7 shows an example of a Nyquist plot of the proposed circuit with $R_1 = R_2 = R_3 = 1\ \Omega$, $C_1 = 0.1$ F, $C_2 = 1$ F and the frequency range of 10 mHz–100 kHz, Fig. 8, on the other hand, shows the Nyquist plot of the circuit with $R_1 = R_2 = R_3 = 1\ \Omega$, $C_1 = 1$ F, $C_2 = 10$ F and frequency range of 1 mHz–100 kHz.

Although the capacitances of the Nyquist plot of Fig. 8 are ten times greater than those in Fig. 7, the Nyquist plots are exactly the same due to different sweeping frequency ranges. This shows that at least the capacitances that are extracted from the Nyquist plots are uncertain and those are dependent to the frequency range. This similarity in the Nyquist plots suggests the use of other impedance plots (e.g. Bode plot) for verifying the extracted equivalent circuit element values. It should also be emphasized that the time constants of the involved processes can be obtained clearly from the Bode phase plot [13].

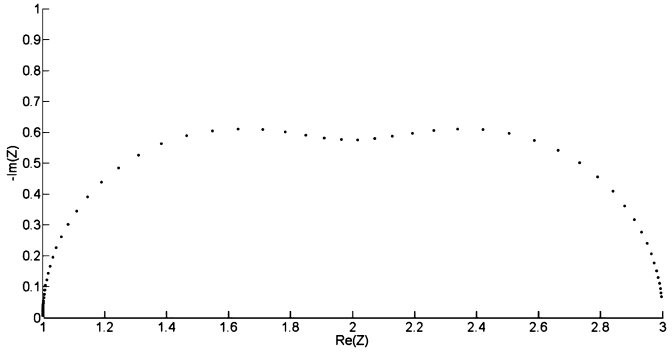

Fig. 7. Nyquist plot with $R_1 = R_2 = R_3 = 1\ \Omega$, $C_1 = 0.1$ F, $C_2 = 1$ F and frequency range of 10 mHz–100 kHz.

There are other examples which have created debates in the literature: for instance, it has been stated that the small semicircle in high frequencies in the Nyquist plot is related to the anode impedance [14,133,134]. However, it has been accepted in the literature that there is a negligible difference between the cathode against the reference electrode and the cathode against the anode electrode [4]. Thus, the small semicircle cannot be due to the anode impedance.

Another debatable topic in the EIS literature is the number of the equivalent circuit elements used to fit to the measured impedance values. It is clear that the more the number of the fitted elements the better the fit between the measured values and the equivalent elements. However, increasing the number of elements does not make the modeling results and predictions better. Furthermore, the measurement models are not determined based on governing equations. Thus, the physical properties of the cell cannot be extracted directly from equivalent circuit elements as has been done in the literature.

7. Summary

The PEM fuel cell studies in recent years using electrochemical impedance spectroscopy (EIS) technique were reviewed in this paper. The EIS method was introduced and some uncommon electrochemistry-based elements in presented equivalent circuits were discussed. Also, the applications of the EIS technique in studying various aspects or parts of the PEM fuel cell were thoroughly reviewed. Modifications and extensions to the classical impedance measurement and hardware were suggested along with debates existed in the EIS-based PEM fuel cell studies. The important points can be summarized as follows:

- The literature emphasizes that the EIS technique can be used to study different aspects of fuel cell structure and performance.
- Most of the studies in application of EIS on fuel cells are classified in the category of measurement models. In these models, the equivalent circuits are suggested based on impedance measurements and there is no direct relation between the proposed equivalent circuit elements and physicochemical properties of the fuel cell, and hence, the physical and

electrochemical interpretations of the values of equivalent circuit elements must be revised.

- The slow reactions and phenomena in fuel cells are related to impedance in low frequency range, and hence, the low frequency range is the most important part of the fuel cell impedance.
- The Nyquist plot consistency with experimental results can be misleading and other impedance plots (e.g. Bode plot) also have to be considered.

References

[1] R. O'hayre, S. Cha, W. Colella, F.B. Prinz, Fuel Cell Fundamentals, second ed., John Wiley & Sons, 2009.
[2] D. Papageorgopoulos, DOE Annual Progress Report, V. Fuel Cells, Fuel Cells Sub-program Overview (2011). http://www.hydrogen.energy.gov/annual_progress11_fuelcells.html.
[3] J. Wu, X.Z. Yuan, H. Wang, M. Blanco, J.J. Martin, J. Zhang, Int. J. Hydrogen Energy 33 (2008) 1735–1746.
[4] X. Yuan, H. Wang, J.C. Sun, J. Zhang, Int. J. Hydrogen Energy 32 (2007) 4365–4380.
[5] P. Agarwal, M.E. Orazem, L.H. Garcia-Rubio, J. Electrochem. Soc. 139 (1992) 1917–1927.
[6] G.J. Brug, A.L.G. Van Den Eeden, M. Sluyters-Rehbach, J.H. Sluyters, J. Electroanal. Chem. 176 (1984) 275–295.
[7] S.M. Rezaei Niya, M. Hejabi, F. Gobal, J. Power Sources 195 (2010) 5789–5793.
[8] P. Gode, F. Jaouen, G. Lindbergh, A. Lundbald, G. Sundholm, Electrochim. Acta 48 (2003) 4175–4187.
[9] F. Jaouen, G. Lindbergh, K. Wiezell, J. Electrochem. Soc. 150 (2003) A1711–A1717.
[10] X.Z. Yuan, J.C. Sun, H. Wang, J. Zhang, J. Power Sources 161 (2006) 929–937.
[11] N.V. Dale, M.D. Mann, H. Salehfar, A.M. Dhride, T. Han, J. Fuel Cell Sci. Technol. 7 (2010) 031010.
[12] M. Cimenti, D. Bessarabov, M. Tam, J. Stumper, ECS Trans. 28 (2010) 147–157.
[13] A. Huth, B. Schaar, T. Oekermann, Electrochim. Acta 54 (2009) 2774–2780.
[14] S.J. Andreasen, J.L. Jespersen, E. Schaltz, S.K. Kaer, Fuel Cells 9 (2009) 463–473.
[15] S.J. Andreasen, J.R. Vang, S.K. Kaer, Int. J. Hydrogen Energy 36 (2011) 9815–9830.
[16] T. Soboleva, X. Xie, Z. Shi, E. Tsang, T. Navessin, S. Holdcroft, J. Electroanal. Chem. 622 (2008) 145–152.
[17] M.A. Danzer, E.P. Hofer, J. Power Sources 183 (2008) 55–61.
[18] M.A. Danzer, E.P. Hofer, J. Power Sources 190 (2009) 25–33.
[19] M. Cimenti, M. Tam, J. Stumper, Electrochem. Solid State Lett. 12 (2009) B131–B134.
[20] I.A. Schneider, S.A. Freunberger, D. Kramer, A. Wokaun, G.G. Scherer, J. Electrochem. Soc. 154 (2007) B383–B388.
[21] I.A. Schneider, D. Kramer, A. Wokaun, G.G. Scherer, J. Electrochem. Soc. 154 (2007) B770–B782.
[22] D. Kramer, I.A. Schneider, A. Wokaun, G.G. Scherer, ECS Trans. 3 (2006) 1249–1258.
[23] G. Maranzana, J. Mainka, O. Lottin, J. Dillet, A. Lamibrac, A. Thomas, S. Didierjean, Electrochim. Acta 83 (2012) 13–27.
[24] B. Legros, P.X. Thivel, Y. Bultel, M. Boinet, R.P. Nogueira, Electrochem. Solid State Lett. 12 (2009) B116–B118.
[25] N. Fouquet, C. Doulet, C. Nouillant, G. Dauphin-Tanguy, B. Ould-Bouamama, J. Power Sources 159 (2006) 905–913.
[26] T. Kurz, A. Hakenjos, J. Kramer, M. Zedda, C. Agert, J. Power Sources 180 (2008) 742–747.
[27] T.E. Springer, T.A. Zawodzinski, M.S. Wilson, S. Gottesfeld, J. Electrochem. Soc. 143 (1996) 587–599.
[28] J. Mainka, G. Maranzana, J. Dillet, S. Didierjean, O. Lottin, FDFC08 (2008). Nancy, France.
[29] J. Mainka, G. Maranzana, J. Dillet, S. Didierjean, O. Lottin, J. Electrochem. Soc. 157 (2010) B1561–1568.
[30] M.U. Iftikhar, D. Riu, F. Drurat, S. Rosini, Y. Bultel, N. Retiere, J. Power Sources 160 (2006) 1170–1182.
[31] M. Bautista, Y. Bultel, P. Ozil, Chem. Eng. Res. Des. 82 (2004) 907–917.
[32] A. Dhanda, H. Pitsch, R. O'Hayre, J. Electrochem. Soc. 158 (2011) B877–B884.
[33] J.E.B. Randles, Discuss. Faraday Soc. 1 (1947) 11–19.
[34] J.E.B. Randles, K.W. Somerton, Trans. Faraday Soc. 48 (1952) 937–950.
[35] D.C. Grahame, J. Electrochem. Soc. 99 (1952) 370C–385C.
[36] D. Malevich, J.G. Pharoah, B.A. Peppley, K. Karan, ECS Trans. 41 (2011) 721–732.
[37] J.H. Jang, S. Jeon, J.H. Cho, S. Kim, S. Lee, E. Cho, H. Kim, J. Han, T. Lim, J. Electrochem. Soc. 156 (2009) B1293–B1300.
[38] A.P. Young, J. Stumper, E. Gyenge, J. Electrochem. Soc. 156 (2009) B913–B922.
[39] Y. Liu, M.W. Murphy, D.R. Baker, W. Gu, C. Ji, J. Jorne, H.A. Gasteiger, J. Electrochem. Soc. 156 (2009) B970–B980.
[40] R. de Levie, Advances in Electrochemistry and Electrochemical Engineering, John Wiley & Sons, 1967.
[41] R. Makharia, M.F. Mathias, D.R. Baker, J. Electrochem. Soc. 152 (2005) A970.
[42] E. Levillain, A. Demortier, J.P. Lelieur, J. Electroanal. Chem. 394 (1995) 103–115.
[43] B.A. Boukamp, H.J.M. Bouwmeester, Solid State Ionics 157 (2003) 29–33.
[44] P. Agarwal, M.E. Orazem, J. Electrochem. Soc. 142 (1995) 4159–4168.
[45] D. Aaron, S. Yiacoumi, C. Tsouris, Separ. Sci. Technol. 43 (2008) 2307–2320.
[46] D. Malevich, E. Halliop, B.A. Peppley, J.G. Pharoah, K. Karan, ECS Trans. 16 (2008) 1763–1774.
[47] D. Malevich, E. Halliop, M.S. Saha, J. Suryana, B.A. Peppley, J.G. Pharoah, K. Karan, 216th ECS Meet. MA2009–02, October 4–9, Vienna, Austria.
[48] C. Brunetto, A. Moschetto, G. Tina, Electr. Power Sys. Res. 79 (2009) 17–26.
[49] J. Hou, W. Song, H. Yu, Y. Fu, L. Hao, Z. Shao, B. Yi, J. Power Sources 176 (2008) 118–121.
[50] J. Hou, H. Yu, M. Yang, W. Song, Z. Shao, B. Yi, Int. J. Hydrogen Energy 36 (2011) I2444–I2451.
[51] A. Pistono, C.A. Rice-York, V. Boovaragavan, J. Electrochem. Soc. 158 (2011) B233–B238.
[52] R. Mukundan, J.R. Davey, R.W. Lujan, J. Spendelow, Y.S. Kim, D.S. Hussey, D.L. Jacobson, M. Arif, R.L. Borup, ECS Trans. 16 (2008) 1939–1950.
[53] I. Nitta, O. Himanen, M. Mikkola, Electrochem. Commun. 10 (2008) 47–51.
[54] J.I. Eastcott, E.B. Easton, Electrochim. Acta 54 (2009) 3460–3466.
[55] J.I. Eastcott, K.M. Yarrow, A.W. Pedersen, E.B. Easton, J. Power Sources 197 (2012) 102–106.
[56] S.J. Seo, J.J. Woo, S.H. Yun, H.J. Lee, J.S. Park, T. Xu, T.H. Yang, J. Lee, S.H. Moon, Phys. Chem. Chem. Phys. 12 (2010) 15291–15300.
[57] S.C. Manzo, P. Rama, R. Chen, J. Electrochem. Soc. 157 (2010) B1865–B1871.
[58] D. Malevich, E. Halliop, B.A. Peppley, J.G. Pharoah, K. Karan, J. Electrochem. Soc. 156 (2009) B216–B224.
[59] S.C. Manzo, P. Rama, R. Chen, J. Electrochem. Soc. 157 (2010) B400–B408.
[60] Z. Tang, D.H.C. Chua, J. Electrochem. Soc. 157 (2010) B868–B873.
[61] T. Kim, S. Yim, Y. Choi, T. Yang, Y. Yoon, S. Park, C. Kim, I. Sung, Electrochem. Commun. 13 (2011) 1313–1316.
[62] P. Mu, W. Qingyu, Int. J. Energy Res. 35 (2011) 923–928.
[63] S. Park, Y. Shao, H. Wan, V.V. Viswanathan, S.A. Towne, P.C. Rieke, J. Liu, Y. Wang, J. Phys. Chem. C 115 (2011) 22633–22639.
[64] S. Park, Y. Shao, R. Kou, V.V. Viswanathan, S.A. Towne, P.C. Rieke, J. Liu, Y. Lin, Y. Wang, J. Electrochem. Soc. 158 (2011) B297–B302.
[65] S. Park, Y. Shao, H. Wan, P.C. Rieke, V.V. Viswanathan, S.A. Towne, L.V. Saraf, J. Liu, Y. Lin, Y. Wang, Electrochem. Commun. 13 (2011) 258–261.
[66] T. Wang, J. He, D. Sun, J. Zhou, Y. Guo, X. Ding, S. Wu, J. Zhao, J. Tang, Corros. Sci. 53 (2011) 1498–1504.
[67] Q. Zheng, X. Cheng, T. Jao, F. Weng, A. Su, Y. Chiang, J. Power Sources 201 (2012) 151–158.
[68] J. Zhang, L. Zhang, C.W.B. Bezerra, H. Li, Z. Xia, J. Zhang, A.L.B. Marques, E.P. Marques, Electrochim. Acta 54 (2009) 1737–1743.
[69] V.C. Velan, G. Velayutham, N. Hebalkar, K.S. Dhathathreyan, Int. J. Hydrogen Energy 36 (2011) 14815–14822.
[70] Y. Bultel, K. Wiezell, F. Jaouen, P. Ozil, G. Lindbergh, Electrochim. Acta 51 (2005) 474–488.
[71] M. Maidhily, N. Rajalakshmi, K.S. Dhathathreyan, Int. J. Hydrogen Energy 36 (2011) 12352–12360.
[72] G. Dotelli, L. Omati, P.G. Stampino, P. Grassini, D. Brivio, J. Power Sources 196 (2011) 8955–8966.
[73] L. Omati, P.G. Stampino, G. Dotelli, D. Brivio, P. Grassini, Int. J. Hydrogen Energy 36 (2011) 8053–8062.
[74] P.G. Stampino, L. Omati, C. Cristiani, G. Dotelli, Fuel Cells 10 (2010) 270–277.
[75] M.C. Lefebvre, R.B. Martin, P.G. Pickup, Electrochem. Solid State Lett. 2 (1999) 259.
[76] T. Kim, S. Lee, H. Park, Int. J. Hydrogen Energy 35 (2010) 8631–8643.
[77] H. Chang, C. Lin, M. Chang, H. Shiu, W. Chang, F. Tsau, J. Power Sources 196 (2011) 3773–3780.
[78] K. Nakagawa, Y. Yasumura, N. Thongprachan, N. Sano, Chem. Eng. Process. 50 (2011) 22–30.
[79] S. Park, B.N. Popov, Fuel 90 (2011) 436–440.
[80] R.P. Ramasamy, E.C. Kumbur, M.M. Mench, W. Liu, D. Moore, M. Murthy, Int. J. Hydrogen Energy 33 (2008) 3351–3367.
[81] S.D. Mikhailenko, M.D. Guiver, S. Kaliaguine, Solid State Ionics 179 (2008) 619–624.
[82] C.H. Lee, H.B. Park, Y.M. Lee, R.D. Lee, Ind. Eng. Chem. Res. 44 (2005) 7617–7626.
[83] P.G. Escribano, C.D. Rio, J.L. Acosta, J. Power Sources 187 (2009) 98–102.
[84] Y. Liu, C. Ji, W. Gu, J. Jorne, H.A. Gasteiger, J. Electrochem. Soc. 158 (2011) B614–B621.
[85] M. Eikerling, A.A. Kornyshev, J. Electroanal. Chem. 475 (1999) 107.
[86] A. Navarro, C.D. Rio, J.L. Acosta, Solid State Ionics 180 (2009) 1505–1510.
[87] M.N. Tsampas, C.G. Vayenas, 217th ECS Meet., 2010, Vancouver, Canada.
[88] M.N. Tsampas, S. Brosda, C.G. Vayenas, Electrochim. Acta 56 (2011) 10582–10592.
[89] M. Keddam, J.-F. Lizee, C. Pallotta, H. Takenouti, J. Electrochem. Soc. 131 (1984) 2016–2024.
[90] I. Epelboin, M. Keddam, Electrochim. Acta 17 (1972) 177–186.
[91] X. Wang, J.-M. Hu, I.-M. Hsing, J. Electroanal. Chem. 562 (2004) 73–80.

[92] C. Lamy, D.J. Jones, C. Coutanceau, P. Brault, S. Martemianov, Y. Bultel, Electrochim. Acta 56 (2011) 10406–10423.
[93] N. Wagner, T. Kaz, K.A. Friedrich, Electrochim. Acta 53 (2008) 7475–7482.
[94] D.C. Martinez-Casillas, G. Vazquez-Huerta, J.F. Perez-Robles, O. Solorza-Feria, J. Power Sources 196 (2011) 4468–4474.
[95] S.S. Pethaiah, G.P. Kalaignan, M. Ulaganathan, J. Arunkumar, Ionics 17 (2011) 361–366.
[96] H. Li, J. Zhang, K. Fatih, Z. Wang, Y. Tang, Z. Shi, S. Wu, D. Song, J. Zhang, N. Jia, S. Wessel, R. Abouatallah, N. Joos, J. Power Sources 185 (2008) 272–279.
[97] H. Li, H. Wang, W. Qian, S. Zhang, S. Wessel, T.T.H. Cheng, J. Shen, S. Wu, J. Power Sources 196 (2011) 6249–6255.
[98] M.J. Martinez-Rodriguez, E.B. Fox, W.D. Rhodes, C.S. McWhorter, S. Greenway, H.R. Colon-Mercado, J. Electrochem. Soc. 158 (2011) B698–B702.
[99] H. Nakajima, T. Konomi, T. Kitahara, H. Tachibana, J. Fuel Cell Sci. Technol. 5 (2008) 041013-1–041013-6.
[100] T. Kadyk, R. Hanke-Rauschenbach, K. Sundmacher, J. Electroanal. Chem. 630 (2009) 19–27.
[101] T. Kadyk, R. Hanke-Rauschenbach, K. Sundmacher, J. Appl. Electrochem. 41 (2011) 1021–1032.
[102] R. Lin, C. Cao, H. Zhang, H. Huang, J. Ma, Int. J. Hydrogen Energy 37 (2012) 4648–4656.
[103] S.K. Roy, H. Hagelin-Weaver, M.E. Orazem, J. Power Sources 196 (2011) 3736–3742.
[104] H. Nara, S. Tominaka, T. Momma, T. Osaka, J. Electrochem. Soc. 158 (2011) B1184–B1191.
[105] F. Xu, L. Zhang, X. Cheng, Y. Zhang, 214th ECS Meet., 2008, Honolulu, HI.
[106] T.A. Aarhaug, A.M. Svensson, A. Odegard, S. Moller-Holst, 215th ECS Meet., MA2009–01, 2009, San Francisco.
[107] F. Sergi, G. Brunaccini, A. Stassi, A. Di Blasi, G. Dispenza, A.S. Arico, M. Ferraro, V. Antonucci, Int. J. Hydrogen Energy 36 (2011) 10908–10916.
[108] D. Seo, J. Lee, S. Park, J. Rhee, S.W. Choi, Y. Shul, Int. J. Hydrogen Energy 36 (2011) 1828–1836.
[109] Y. Cho, T. Jeon, J.W. Lim, Y. Cho, M. Ahnb, N. Jung, S. Yoo, W. Yoon, Y. Sung, Int. J. Hydrogen Energy 36 (2011) 4394–4399.
[110] Y. Cho, S. Kim, J.W. Lim, Y.S. Kang, Y. Cho, O. Kim, N. Kwon, O.J. Kwon, W. Yoon, H. Choe, Y. Sung, Int. J. Hydrogen Energy 37 (2012) 2490–2497.
[111] S.K. Roy, M.E. Orazem, J. Power Sources 184 (2008) 212–219.
[112] S.K. Roy, M.E. Orazem, J. Electrochem. Soc. 156 (2009) B203–B209.
[113] I.A. Schneider, M.H. Bayer, A. Wokaun, G.G. Scherer, J. Electrochem. Soc. 155 (2008) B783–B792.
[114] S. Rodat, S. Sailler, F. Druart, P.-X. Thivel, Y. Bultel, P. Ozil, J. Appl. Electrochem. 40 (2010) 911–920.
[115] O.J. Kwon, M.S. Kang, S.H. Ahn, I. Choi, K.U. Lee, J.H. Jeong, I. Han, J.C. Yang, J.J. Kim, Int. J. Hydrogen Energy 36 (2011) 9799–9804.
[116] J. Mainka, G. Maranzana, J. Dillet, S. Didierjean, O. Lottin, WHEC-2010 (2010, May 16–21). Essen.
[117] S. Asghari, A. Mokmeli, M. Samavati, Int. J. Hydrogen Energy 35 (2010) 9283–9290.
[118] A.M. Dhirde, N.V. Dale, H. Salehfar, M.D. Mann, T.H. Han, IEEE Trans. Energy Convers. 25 (2010) 778–786.
[119] X. Yuan, J.C. Sun, H. Wang, H. Li, J. Power Sources (2012), http://dx.doi.org/10.1016/j.jpowsour.2012.01.039.
[120] J. Juang, Applied System Identification, Prentice Hall, New Jersey, 1994.
[121] S.K. Roy, M.E. Orazem, ECS Trans. 13 (2008) 153–169.
[122] M. Jung, M.D. Ashford, K.A. Williams, Fuel Cells 11 (2011) 327–338.
[123] S. Wasterlain, F. Harel, D. Candusso, D. Hissel, X. Francois, J. Fuel Cell Sci. Technol. 8 (2011) 024502.
[124] A. Bergmann, T. Kurz, D. Gerteisen, C. Hebling, WHEC 2010 Book 1 (2010).
[125] M.A. Rubio, A. Urquia, R. Kuhn, S. Dormido, J. Power Sources 183 (2008) 118–125.
[126] M.A. Rubio, A. Urquia, S. Dormido, Int. J. Hydrogen Energy 35 (2010) 2586–2590.
[127] J. Deseure, J. Power Sources 178 (2008) 323–333.
[128] L.D. Schmidt, The Engineering of Chemical Reactions, Oxford Univ. Press, 1998.
[129] J. O'Rourke, M. Ramani, M. Arcak, Int. J. Hydrogen Energy 33 (2008) 4694–4701.
[130] K. Pattamarat, M. Hunsom, Korean J. Chem. Eng. 25 (2008) 245–252.
[131] A.J. Bard, L.R. Faulkner, Electrochemical Methods, Fundamentals and Applications, second ed., John Wiley & Sons, 2001.
[132] J. Le Canut, R. Latham, W. Merida, D.A. Harrington, J. Power Sources 192 (2009) 457–466.
[133] A. Iranzo, M. Munoz, F.J. Pino, F. Rosa, J. Power Sources 196 (2011) 4264–4269.
[134] J. Lee, J. Lee, W. Choi, K. Park, H. Sun, J. Oh, J. Power Sources 195 (2010) 6001–6007.